

Volumetric curvature attributes adding value to 3D seismic data interpretation

Satinder Chopra* and Kurt J. Marfurt⁺

*Arcis Corporation, Calgary; ⁺University of Houston, Houston

Summary

During the last few years, curvature attributes have been found to be useful for delineating faults and predicting fracture orientation and distribution. In addition to structural features, curvature can also help in illuminating channels, levees, reef edges, and collapse features. There are different curvature measures that can be used, each having its own characteristic property. Originally developed for explicit application to explicitly picked horizons, curvature computations can now be applied to seismic volumes through intermediate calculations of volumetric dip and azimuth. The orientations of faults and fracture lineaments interpreted on curvature displays can be combined in the form of rose diagrams, which in turn can be compared with similar diagrams obtained by FMI well logs to gain confidence in calibration.

Introduction

Horizon-based curvature attributes (Roberts, 2001) have been used in seismic data interpretation for predicting fractures ever since Lisle (1994) demonstrated the correlation of curvature values to fractures measured on an outcrop. Different measures of curvature (Gaussian, strike, dip, etc...) have been shown by different workers to be highly correlated with fractures (Hart, 2002; Ericsson et al., 1988; Sigismondi and Soldo, 2003); Chopra and Marfurt (2007b) summarize much of this work. By definition, all such applications need the interpretation of a seismic horizon, which may be a simple task should the data quality be good and the horizon of interest corresponds to a prominent impedance contrast. In contrast, horizons picked from noisy seismic data contaminated by backscattered noise and/or acquisition footprint, or when picked through regions where no consistent impedance contrast exists, can lead to inferior curvature measures. One partial solution to noisy picks is to run a spatial filter over them, taking care to remove the noise yet retain the geometric detail. (Hesthammer, 1999; Chopra and Marfurt, 2006).

Al Dossary and Marfurt (2006) extended the Bergbauer et al.'s (2003) multispectral analysis of curvature to seismic volumes. This volumetric estimation of curvature alleviates the need for picking horizons in regions through which no continuous surface exists. This paper reports the results of our investigations into both horizon-based and volumetric curvature attribute applications. Even after careful spatial filtering, horizon-based curvature estimates may still suffer from artifacts. Curvature attribute values extracted from curvature attribute volumes along the same set of horizons yields displays that are free of artifacts and make more geologic sense.

Attributes and structure-oriented filtering

The goal of structure-oriented filtering is to apply well-established filters along the dip and azimuth of seismic reflectors and in so doing remove noise and enhance lateral continuity. Structure-oriented filtering discriminates between signal that is aligned with the estimated reflector dip and azimuth and random or coherent noise that crosses it in some other direction. Once the dip/azimuth has been estimated, a filter can be applied to enhance signal along the reflector, much as interpreters do with time/structure and amplitude extraction maps using interpretation workstation software. The familiar ones are the mean, median and α -trim (Chopra and Marfurt, 2007a). While these filters do a good job in enhancing the signal-to-noise ratio of the data, they often smear the faults.

Hocker and Fehmers (2002) address this problem by using an 'anisotropic diffusion' smoothing algorithm. The 'anisotropic' part of anisotropic diffusion is so named in that the smoothing takes place parallel to the reflector, while no smoothing takes place perpendicular to the reflector. Most important, no smoothing takes place if a discontinuity is detected, thereby preserving the appearance of major faults and stratigraphic edges. Luo et al.'s (2002) edge-preserved filtering proposed a competing method that uses a multiwindow (Kuwahara) filter to address the same problem. Both these approaches use a mean filter or median filter applied to data values that fall within a spatial analysis window one sample thick.

Marfurt (2006) describes a multiwindow (Kuwahara) principle component filter that uses a vertical window of data samples to compute the waveform that best represents the seismic data in the spatial analysis window. Seismic processors may be more familiar with the principal component filter as the equivalent Kohonen-Loeve (or simply KL) filter. In this work, we use ninety-nine 9-trace, ± 10 ms (11 sample) analysis windows oriented parallel to the dip/azimuth that contain the analysis point of interest. We then apply our principal component filter to the analysis point using that window that has the most coherent data within it. Because it uses (for our examples 11 times) more data, the pc filter in general produces significantly better results than the corresponding mean filter. We admonish the hopeful reader that there is no such thing as a 'silver bullet' in seismic data processing. If the data are contaminated by high amplitude spikes, a median, alpha-trim mean, or other nonlinear filter will provide superior results. Likewise the pc-filter will preserve amplitude variations in coherent signal that may be due to the acquisition geometry whereas a mean filter will smooth them out.

Seismic data that has been subjected to pc filtering will in general have higher a signal-to-noise ratio, exhibit sharper discontinuities, and provide enhanced images of faults, fractures and stratigraphic features such as channels. We show the application of pc filtering on a seismic dataset from Alberta in Figure 1. Notice not only the overall cleaner look of the section after pc filtering, but the sharpening of the vertical faults as well. Attributes computed from seismic data that have a good signal-to-noise ratio are bound to yield significantly more meaningful geologic information.

Curvature images of differential compaction over channels

Figure 2a shows a time-structure map interpreted from a 3D seismic surface acquired in Alberta, Canada. This horizon was the nearest continuous event above a slightly deeper channel system of interest. We manually picked a grid of control lines, then autotracked the horizon, and then applied a 3 x 3 mean filter to remove short wavelength jitter from the interpreted picks. Next, we computed the most-positive and most-negative curvature directly from the horizon to generate the horizon-based curvature images displayed in Figure 2b. Notice both these displays are contaminated by a time contour overprint, as indicated by the cyan, blue and grey arrows. Such overprints are artifacts that do not make any geologic sense. We do not see any clear evidence of the channel system below this horizon.

Next we computed volumetric estimates of most positive and most negative curvature corresponding to every sample in the seismic volume and display horizon slices through both attribute volumes in Figures 2d and e. Not only are Figures 2d and e free of the time contour artifacts seen in Figures 2b and 2c, but also depict some of the limbs of a shallower channel system, indicated by the block arrows. We see these deeper channels due to differential compaction between the sediments that fill the channels and the matrix through which they cut.

In Figure 2f, we display phantom horizon slices 36 ms above the picked time surface displayed in Figure 2a and also indicate the position and show segments of the inline (Figure 2g) and crossline (Figure 2h) seismic sections passing through it. Points AA' and BB' indicate the edges of the main circular channel on the inline and crossline sections. In Figures 2i, j and k we show the coherence, most-positive curvature and most-negative curvature attributes extracted along this horizon. Notice the clarity with which the channel system stands out, with the main limb running NW-SE and the other limbs showing the deltaic distribution on both sides. Because of differential compaction and the potential deposition of levies, the most negative curvature highlights the channel axis or thalweg, while the most positive curvature defines the flanks of the channels and potential levee and overbank deposits. The coherence images are complementary and are insensitive to differential compaction; rather it highlights those

areas of the channel flanks where we have a lateral change in waveform.

The value of volumetric attributes are two-fold. First, as shown in Figures 2d and e, our images have higher signal-to-noise. Volumetric estimates of curvature are computed not from one picked seismic sample, but rather from a vertical window of seismic samples (in our case, 11 samples), such that they are statistically less sensitive to backscattered noise. Second, not every geologic feature that we wish to interpret falls along a horizon that can be interpreted, such as the channel system shown here. While we could interpolate horizon-based curvature computed above and below our channel system, such an interpolated image would be significantly less sensitive to the rapid geomorphological changes we see in the vertical section.

Curvature images of faults and fractures

In addition to the channel feature definitions, such displays would help in bringing out the definition of subtle faults and fractures that may help in the placement of horizontal wells.

All attribute interpretations on time and horizon slices should be validated through inspection of the vertical seismic data. In Figure 3 we show a zoom of the time slices through coherence, most-positive and the most-negative curvature volumes intersecting a seismic inline. Notice, how the red peaks (Figure 3b) on the fault lineaments (running almost north-south) correlate with the upthrown signature on seismic. Similarly, the most-negative curvature time-slice intersecting with the seismic inline (Figure 3c) shows the downthrown edges on both sides of the faults highlighted in blue.

Curvature attributes for well-log calibration

Figure 4a shows a horizon slice extracted from the most-positive curvature volume at a level 30 ms below a horizon time surface from a 3D seismic volume from central-north British Columbia, Canada. A number of faults can be seen on the vertical seismic section. The individual lineaments corresponding to the two main faults running north-south as well as their fracture offshoots have been tracked in yellow color. The orientations of these lineaments have been combined in the form of a rose diagram shown in Figure 4b, retaining the color of the lineaments. This rose diagrams can be compared with a similar diagram obtained from FMI (Formation Micro-Imager) wells log to gain confidence in calibration. Once a favourable match is obtained, the interpretation of fault/fracture orientations and the thicknesses over which they predominate can be trusted for a more quantitative analysis, which in turn could prove useful for production from reservoirs.

Conclusions

Curvature attributes are a useful set of attributes that measure lateral changes in dip and azimuth and augment attributes that are sensitive to lateral changes in

waveform (such as coherence) and amplitude (such as Sobel filters). Being second order derivative measures of surfaces, they are sensitive to noise. On time surfaces picked on noisy data, noise on picks can be attenuated by iteratively running spatial filtering. For volume computation of attributes, structure-oriented filtering often does a satisfactory job. Volume curvature attributes provide valuable information on fracture orientation and density in zones where seismic horizons are not trackable. The orientations of the fault/fracture lineaments interpreted on curvature displays can be combined in the form of rose diagrams, which in turn can be compared with similar diagrams obtained from FMI (Formation Micro-Imager) wells logs to gain confidence in calibration.

Acknowledgements

We thank Arcis Corporation for permission to show the data examples and publish this work.

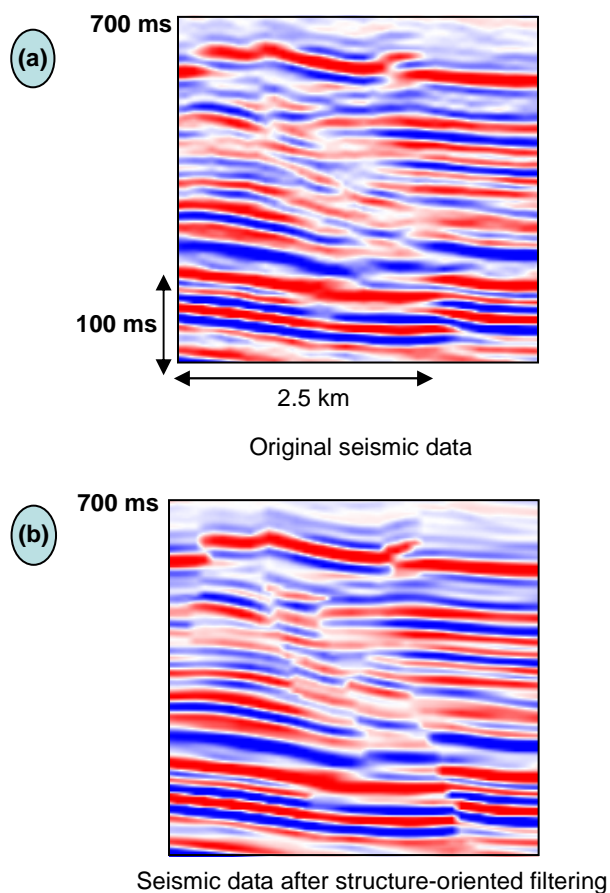
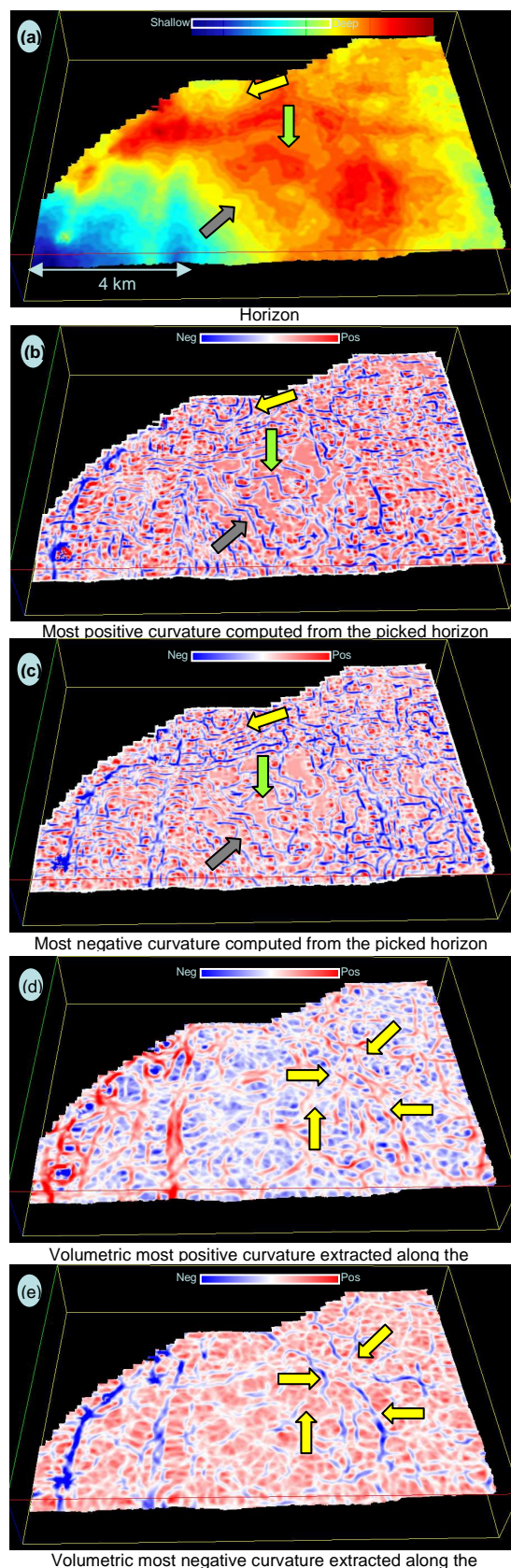


Figure 1: Two segments of a seismic section (a) before and (b) after the application of pc-filtering from a 3D seismic volume from Alberta, Canada. Notice the cleaner background and focused amplitudes of the seismic reflections after pc-filtering as well as the preserved fault edges. Data courtesy of Arcis Corporation, Calgary.



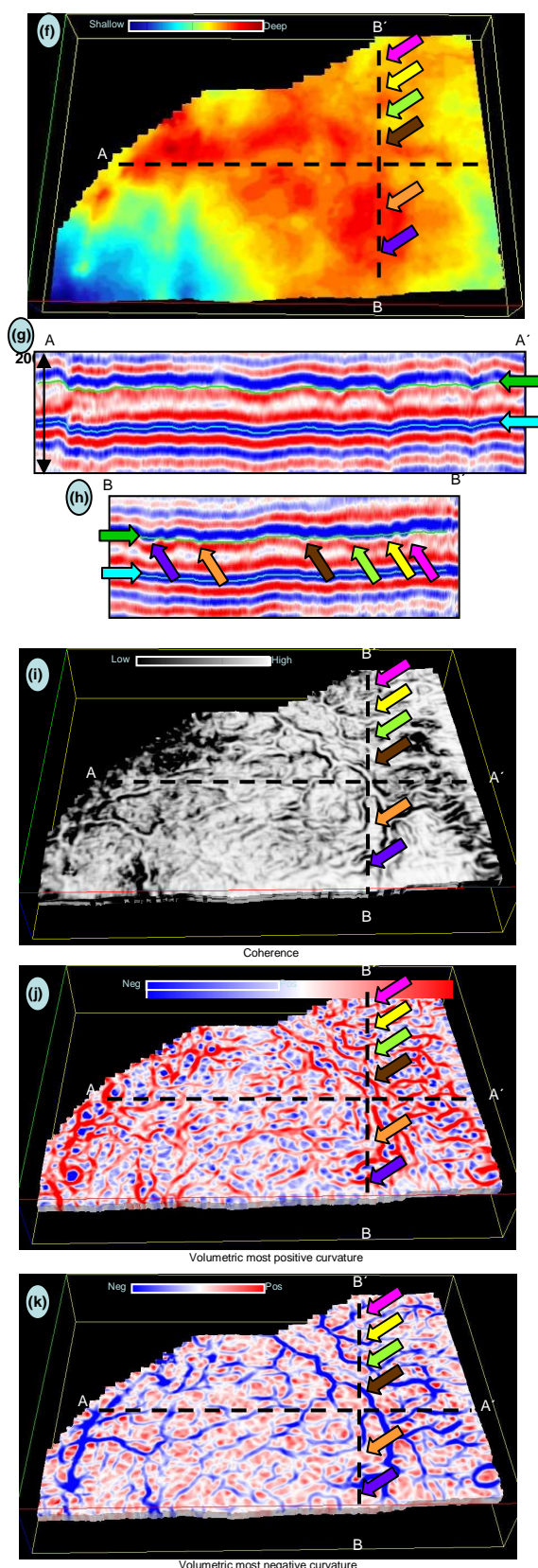


Figure 2: (a) Time surface from a 3D seismic data volume from Alberta, (b) most-positive curvature display for the time surface in (a), (c) most-negative curvature display for the time surface in (a), (d) most-positive curvature display extracted from the attribute volume along the time surface in (a), (e) most-negative curvature display extracted from the attribute volume along the time surface in (a), (f) time surface from the same seismic volume but 36 ms above the time surface in (a), (g) segment of a seismic crossline cutting the circular part of the main channel on the time surface in (f), (h) segment of a seismic inline cutting the circular part of the main channel on the time surface in (f), (i) coherence horizon slice (j) most-positive (k) most-negative attribute horizon slices corresponding to the time surface shown in (f). Data courtesy of Arcis Corporation, Calgary.

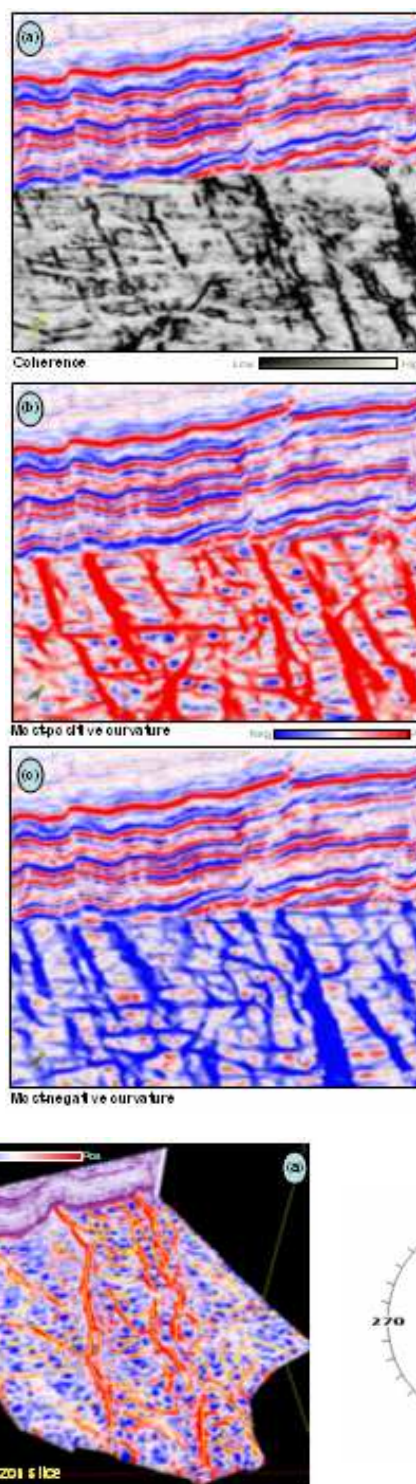


Figure 3: Zoom of chair-displays where the vertical display is an inline from the 3D seismic volume and the horizontal displays are time slices from (a) coherence (b) most-positive (c) most-negative. The fault lineaments correlate with the upthrown and downthrown signatures on the seismic. Data courtesy of Arcis Corporation, Calgary.

Figure 4: (a) lineaments corresponding to the faults marked as yellow lines, (b) orientations of the marked lineaments (yellow) in (c) combined in the form of a Rose diagram. Data courtesy of Arcis Corporation, Calgary.

EDITED REFERENCES

Note: This reference list is a copy-edited version of the reference list submitted by the author. Reference lists for the 2007 SEG Technical Program Expanded Abstracts have been copy edited so that references provided with the online metadata for each paper will achieve a high degree of linking to cited sources that appear on the Web.

REFERENCES

- Al-Dossary, S., and K. J. Marfurt, 2006, Multispectral estimates of reflector curvature and rotation: *Geophysics*, 71, no. 5, P41–P51.
- Bergbauer, S., T. Mukerji, and P. Hennings, 2003, Improving curvature analyses of deformed horizons using scale-dependent filtering techniques: *AAPG Bulletin*, 87, 1255–1272.
- Blumentritt, C. H., 2006, Volume based curvature analysis illuminates fracture orientations: Presented at the Annual Meeting, AAPG.
- Chopra, S., and K. J. Marfurt, 2007a, Curvature attribute applications to 3D seismic data: *The Leading Edge*, 26, 404–414.
- , 2007b, Seismic attributes for prospect identification and reservoir characterization: SEG.
- Chopra, S., K. J. Marfurt, and V. Alexeev, 2006, Practical aspects of curvature computations from seismic horizons: 76th Annual International Meeting, SEG, Expanded Abstracts, 1712–1715.
- Cooper, G. R. J., and D. R. Cowans, 2003, Sunshading geophysical data using fractional order horizontal gradients: *The Leading Edge*, 22, 204–205.
- Ericsson, J. B., H. C. McKeon, and R. J. Hooper, 1988, Facies and curvature controlled 3-D fracture models in a Cretaceous carbonate reservoir, Arabian Gulf, in G. Jones, Q. J. Fisher, and R. J. Knope, eds., *Faulting, fault sealing and fluid flow in hydrocarbon reservoirs*: Geological Society Special Publication, 147, 299–312.
- Hart, B. S., 2002, Validating seismic attributes: Beyond statistics: *The Leading Edge*, 21, 1016–1021.
- Hesthammer, J., 1999, Improving seismic data for detailed structural interpretation: *The Leading Edge*, 18, 226–247.
- Hoecker, C., and G. Fehmers, 2002, Fast structural interpretation with structure-oriented filtering: *The Leading Edge*, 21, 238–243.
- Lisle, R. J., 1994, Detection of zones of abnormal strains in structures using Gaussian curvature analysis: *AAPG Bulletin*, 78, 1811–1819.
- Luo, Y., S. Al-Dossary, and M. Alfaraj, 2002, Edge-preserving smoothing and applications: *The Leading Edge*, 21, 136–158.
- Marfurt, K. J., 2006a, Robust estimates of reflector dip and azimuth: *Geophysics*, 71, no. 4, P29–P40.
- , 2006b, Seismic attribute mapping of structure and stratigraphy: DISC Course, SEG/EAGE.
- Roberts, A., 2001, Curvature attributes and their application to 3D interpreted horizons: *First Break*, 19, 85–99.
- Sigismondi, E. M., and C. J. Soldo, 2003, Curvature attributes and seismic interpretation: Case studies from Argentina basins: *The Leading Edge*, 22, 1122–1126.